2012

Evaluation Of Defrost Options For Secondary Coolants In Multi-temperature Indirect Transport Refrigeration: Mathematical Modelling & Sensitivity Analysis

Donal Patrick Finn
donal.finn@ucd.ie

Andreas Cabello-Portoles

Shane Smyth

Barry Brophy

Evaluation of Defrost Options for Secondary Coolants in Secondary Loop Multi-temperature Transport Refrigeration Systems - Mathematical Modelling & Sensitivity Analysis

Donal P. FINN[1*], Andreas CABELLO-PORTOLES[2], Shane SMYTH[3] and Barry BROPHY[4]

[1]School of Mechanical & Materials Engr., University College Dublin, Dublin, Ireland,
Tel: +353 1 716 1947 Fax: + 353 1 283 0534 Email: donal.finn@ucd.ie

[2]Escuela Técnica Superior de Ingenieros Industriales, Universidad Politécnica de Valencia, Spain
Tel: +34 91 336 30 60 Fax: +34 91 561 86 18 Email: andrcarpor@etsii.upv.es

[3]ThermoKing Ltd., Monivea Road, Galway, Ireland.
Tel: +353 91 703 384 Fax: +353 91 703 273 Email: ssmyth@irco.com

[4]School of Mechanical & Materials Engr., University College Dublin, Dublin, Ireland,
Tel: +353 1 716 1737 Fax: +353 1 283 0534 Email: barry.brophy@ucd.ie

* Corresponding Author

ABSTRACT

This paper describes a mathematical model of the defrost process for a finned-tube air chiller, utilised as a heat exchanger in a secondary loop multi-temperature transport refrigeration system, where an antifreeze mixture is deployed as a sensible secondary working fluid. Two defrost modes are modeled: an electric mode which effects defrost by localised resistance heating of the chiller secondary working fluid, and a hot gas primary circuit mode that indirectly heats the secondary working fluid by means of a primary to secondary heat exchanger. The model, which was implemented using the Engineering Equation Solver (EES), is based on a finite difference approach to analyse the heat transfer from the secondary working fluid, through a single finned heat exchanger section, to the frost. An iterative scheme is used to integrate for the overall heat exchanger, taking into account temperature glide associated with the secondary working fluid. The overall heat exchanger model is incorporated within a system defrost model, which allows the entire defrost process to be modeled. The model was validated for the standard United Nations Agreement on Transportation of Perishable Produce (ATP) for cold room set-points of 0^{o}C, -10^{o}C and -20^{o}C, by comparison with experimental data from a full scale laboratory based test programme. The validated model is used to carry out defrost sensitivity studies which examine defrost behavior for a range of performance parameters.

1. INTRODUCTION

The use of secondary working fluids, in conjunction with secondary loop refrigeration (IDX) system design, is gaining increased interest for certain applications, as an alternative approach to direct expansion (DX) systems. This is particularly so, where long refrigerant pipe runs and refrigerant charges are required. In the past decade, there is increased evidence, of the successful deployment of secondary loop systems in supermarket and storage applications, where their use can offer advantages including: reduced refrigerant charge (Horton and Groll, 2003), better control (Kazachki and Hinde, 2006) and improved reliability (Hinde et al., 2009). Other research has examined associated component optimisation issues with IDX systems such as: heat exchangers (Haglund-Stignor, 2007), secondary working fluids (Melinder, 1997, Aittomaki and Lahti, 1997, Sawalha and Palm, 2003) and pumping power (Kazachki and Hinde, 2006). As with DX systems, defrosting of the chillers is a key operational issue in IDX system design and is the subject matter of the current paper. A mathematical model of the defrost process in a finned-tube air chiller, utilised as a heat exchanger in a secondary loop multi-temperature transport refrigeration system, where an antifreeze mixture is deployed as a secondary working fluid is described. Two defrost modes are modeled; an electric defrost mode which effects defrost by localised resistance heating of the secondary working fluid and a hot gas primary circuit defrost, that indirectly heats the secondary working fluid by means of a primary to secondary heat exchanger. The defrost model, which is implemented using the Engineering Equation Solver (EES 2008), is based on adapting a finite difference approach outlined originally by Hoffenbecker (2004) for a DX chiller. The current model, adapted for an IDX system, describes the heat transfer from the secondary working fluid, through a single heat exchanger fin section and associated melting of the accumulated frost. The defrost model is integrated for the entire heat exchanger to account for the temperature glide of the secondary working fluid and is incorporated within a model of the secondary system circuit to give an overall system defrost model. The model is validated according to the United Nations Agreement on Transportation of Perishable Produce procedure for cold room set-point temperatures of 0^{o}C, -10^{o}C and -20^{o}C, by

comparison with experimental data from the full scale laboratory based test programme (ATP, 2003). The contribution of the current paper is that it examines the performance of two defrost modes in a secondary loop refrigeration system which to date has not been examined for IDX systems in transport refrigeration.

2. LITERATURE REVIEW

Alebrahim and Sherif (2002) summarise the range of defrost options that are typically available for the melting of frost from evaporator coils. These include: hot gas bypass, reverse cycle operation, electric resistance heating, warm liquid defrost and self-defrosting by evaporator or system shutdown. Because of their relative simplicity and effectiveness, hot gas and reverse cycle defrosting are the most pervasive defrost modes in DX systems, followed by direct resistance heating of the evaporator coil.. Krakow et al. (2003) outline the defrost process in a typical DX evaporator. Defrost can be characterised by subdividing it into four stages as follows: preheating, melting, vaporizing and dry heating. On the refrigerant side, the defrost process is subdivided into three stages: a rapid equalization stage, a transfer stage and a continuous flow stage. Hoffenbecker (2004, 2005) describes the development of a transient finite difference model for predicting the heat and mass transfer effects associated with an industrial air-cooling direct expansion evaporator during a hot gas defrost cycle. The model inputs include the chamber dry bulb temperature and humidity, the coil geometry, the frost thickness and density and hot gas inlet temperature. The model predicts the time required for complete frost melting as well as the sensible and latent loads transferred to the conditioned space during defrost. The model was validated by comparing predicted results to actual defrost cycle field measurements as well as with data in previously published studies (Niederer 1976). Alebrahim and Sherif (2002) describe a mathematical model for the transient simulation of an electric defrost process in a direct expansion evaporator. In their paper, they outline the application of an enthalpy finite difference method, which describes the heat transfer through a repeating frosted evaporator section. The method deployed incorporates a number of advantages, including; its ability to handle the phase change associated with the frost melt process, the transient nature of the defrost process, as well providing flexibility to deal with variable initial and complex boundary conditions. Liu describes the dynamic simulation of hot-gas defrost process in an air source heat pump evaporator. The defrost model is based on a distributed model of the evaporator and considers sensible and latent energy associated with the defrost process, as well as parasitic losses due to convection and evaporation to the evaporator chamber. Good agreement was found between simulation predictions and experimental results for one defrost study (Liu 2003). Mei (2002) presents analysis of a warm liquid defrost utilised on a supermarket display case system. It is noted that there are many advantages associated with this approach including quick frost removal with avoidance of the hot gas lines as required by the hot gas defrost systems, with less refrigerant charge than hot gas systems, a reduction in thermal shock to the evaporators, reduction in heat transferred to the cold air in the display case and improved defrost energy efficiency.

3. MATHEMATICAL MODEL

3.1 Overview

The mathematical model developed in this work can be subdivided into three components as follows: (a) a fin and tube model, (b) a chiller heat exchanger model and, (c) a defrost circuit model. The fin and tube model is based on an adaptation of a finite difference approach, similar to Hoffenbecker (2005), to model the heat transfer from the secondary working fluid, through the fin section to the frost. In the current model, as a sensible secondary working fluid rather than a condensing gas is considered, a temperature glide is taken into account, resulting in discretization of the chiller into a series of independent nodes. Finally the chiller model is incorporated with a model of the pipe transportation and defrost heat input, thereby providing the overall defrost model, as summarised in Figure 1.

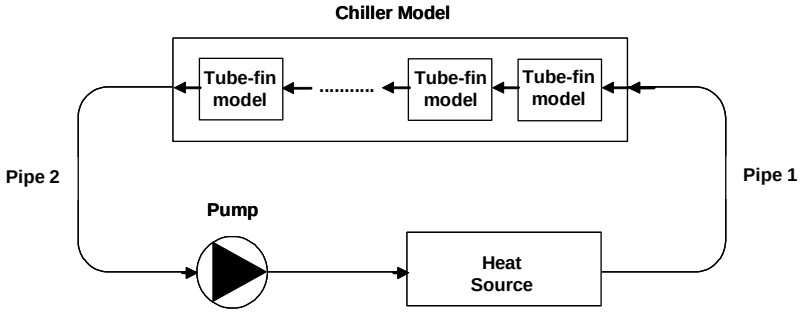

Figure 1: Defrost System Schematic

In the current work, the cross flow heat exchanger as shown in in Figure 2, consists of 3 passes, each of which consists of 36 flow traverses per pass. This results in each pass consisting of a single throughput of length 21.6 m, with 141 fin plates. As no surface enhancement were present on the fin or tube surfaces, such effects were not modeled..

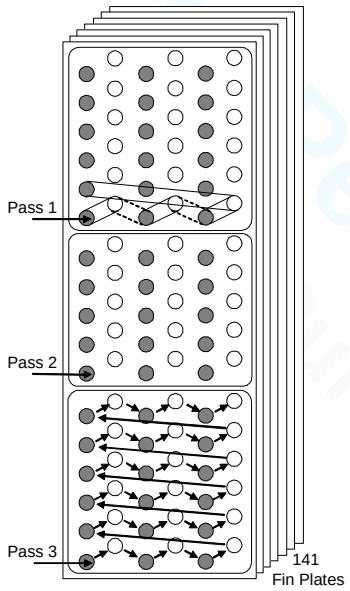

Chiller Parameter	Data
Fin Plate Dimensions (mm)	182 x 560
Fin Thickness (mm)	0.25
Fin Spacing (mm)	5.0
No. of Fins	114
Heat Transfer Surface Area (m^2)	23.8
Coil Parameter	**Data**
Secondary Fluid Passes	3
Pass Length (m)	21.6
Circuit tube external diameter (mm)	13
Circuit tube internal diameter (mm)	12
Tube vertical pitch (mm)	
Tube horizontal pitch (mm)	12

Figure 2: Heat Exchanger Specification

3.1 Fin and Tube Model

Hoffenbecker (2005) modeled defrost in a cross flow heat exchanger, subject to a condensing hot gas, by utilising a fin section to model heat transfer from the hot gas to the frost. The fin section is based on a single tube surrounded by an annular fin section. The fin is assumed to be covered with frost, and this allows an axisymmetric assumption to be applied. The frosted fin combination is modeled by application of a 12 node finite difference grid in the axial and radial directions. In the current fin-tube fin model, a similar approach used for the heat transfer process from the secondary working fluid to the frost. In order to simplify the analysis, each hexagonal fin area was approximated and modelled as an annular fin, where it is assumed that an annular fin is considered to be a symmetrical repeating section. If a single fin is examined, it can be seen from Figure 3(a), that the symmetry of the fin surrounding each tube resembles a hexagon, whereupon the multiple hexagonal areas are used to approximate a single fin of an evaporator. Moreover, each hexagonal area can be approximated as an annular fin as shown in Figure 3(a). Like the hexagonal area around each chiller tube, the annular fin area profile can also be used to approximate a single evaporator fin. Applying symmetry, a typical tube in the chiller with its attached fin forms the basis for establishing a model of the defrost process. Figure 3(a) shows an isolated portion of the chiller coil after applying symmetry, considering only a half of the tube-fin assembly (with frost) and the approximation of a circular fin from the hexagon when the frost builds up on the fin surface.

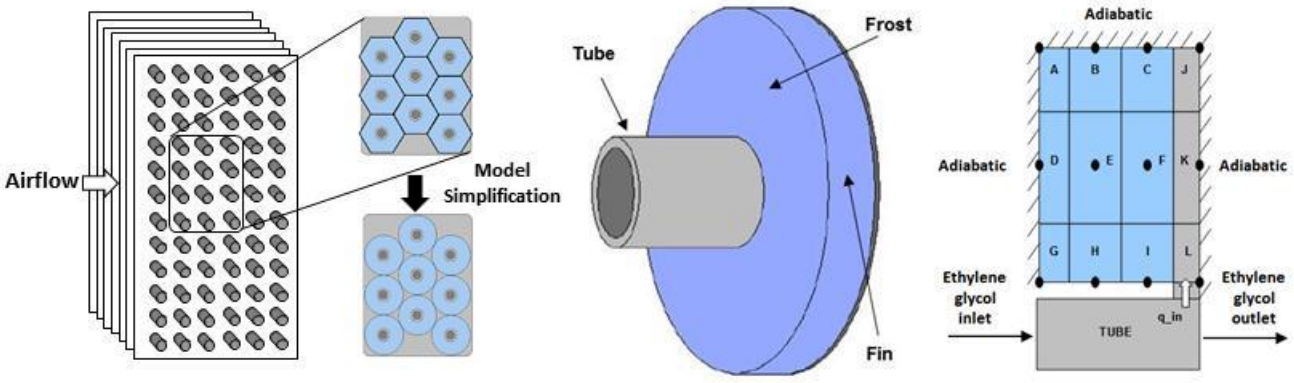

Figure 3: (a) Fin tube bundle utilised in the current work, (b) geometric assumption of fin tube bundle and (c) discritisation approach (after Hoffenbecker 2005).

3.2 Model Grid Independence

The grid size was set by carrying out a sensitivity study for different fin-frost grid densities. This was achieved by assuming a uniform circumferential heat flux along the tube boundary. Table 1 summarises the relative difference in simulated defrost time relative to a 10 x 10 mesh. This sensitivity study was carried out for a 2.5 kW load with a chamber setpoint of -20^{o}C. A frost mesh size from a 4 x 3 to a 10 x 10 grid was considered. In addition, the number of circuit nodes was varied from 1 to 10. This gave a variable matrix which varied from 4132 variables associated with the 10 x 10 x 10 grid, to 211 variables associated with the 4 x 3 x 2 grid. An explicit finite difference model was used to determine the required time step, which varied from 1 second for the 4 x 3 x 2 grid to 0.01 seconds for the 10 x 10 x 10 grid. Utilising a minimum relative different tolerance of 5% compared to the finest model size proposed, a grid size of 4 x 3 x 10 was chosen for the frost-fin mesh (see Fig. 3(b)), since the calculation time required for the simulation increases significantly as the mesh size increases, without necessarily giving significant solution improvement.

Table 1: Error associated with different model grid specifications

Error depending on the model size		Frost - fin mesh size		
		4 x 3	6 x 6	10 x 10
Number of circuit nodes	2	7.01 % (211 - 1)	5.12 % (400 - 0.1)	2.53 % (908 - 0.01)
	5	5.13 % (406 - 1)	3.02 % (865 - 0.1)	0.8 % (2117 - 0.01)
	10	4.34 % (731 - 1)	2.55 % (1640 - 0.1)	0 % (4132 - 0.01)

3.3 Chiller Model

The entire chiller consists of 48 independent circuits, which are subdivided into N tubes and n passes. Each of the circuits is considered to be independent, so the temperature of the glycol at the inlet and at the outlet each is assumed to be the same, thereby reducing the problem to the analysis of a single circuit.

3.4 System Defrost Model

The system defrost model consists of a number of components as outlined in the following sections.

3.4.1 Chiller & Fins: The air chillers are comprised of a series of tubes with fins attached to their exterior surfaces to provide an extended heat transfer area. The tubes are grouped into circuits, which represent the way the secondary working fluid passes through the chiller.

3.4.2 Power Supply: The power supply configuration depends on the defrost mode. For electric defrost, electric resistance heating is used; which is measured using a power meter. In the case of hot gas defrost, a plate heat exchanger couples the secondary working fluid (glycol) to the hot gas of the primary cycle, where the compressor power is measured. In both cases, the same circulation pump (Maximum rating = 375 W) is used to circulate the secondary working fluid to the cold room. The associated power consumption was found to be similar for both cases and is not included in the overall power used for the defrost process.

3.4.3 Circuit: Two circuits which connect the power supply with the chiller are modelled using a finite difference approach, where they are subdivided into several nodes. Axial discretization is applied by taking into account the required step time for time integration.

For the finite difference model, a time step for the integration to satisfy two convergence criteria was chosen, one for energy transport in the pipes and the other for the fin-tube model. Based on these convergence criteria, a time step of 1 second was utilised. Any heat losses to the surroundings were ignored.

3.5 Model Inputs and Outputs

The main inputs of the model are: (i) the amount of frost present on the chiller, (ii) the initial conditions of the system, (iii) the power used to heat the secondary refrigerant. The model predicts: (i) the time required to complete the defrost, (ii) the distribution of energy put in the system, (iii) the evolution of the temperatures of the secondary refrigerant and (iv) the defrost efficiency. The defrost efficiency is defined as the amount of energy that is required to melt the frost on the heat exchanger with respect to the total energy supplied to the chiller for a defrost cycle. It should be noted that the energy required to melt the frost represents only some of the stored energy of the frost, since the rest of the stored energy is used to raise the temperature of the frost nodes above 0 ºC.

4. MODEL VALIDATION

Validation was carried out for the model in electric mode and hot gas mode for nine different test conditions as outlined in Table 2.

4.1 Electric Defrost

Figure 4 compares the evolution of the glycol temperatures and flowrates for model predictions against experimental data for a coldroom setpoint of -20°C, for two heat input rates, 0.5 kW and 2.5 kW. Similar results were also found for the 1.5 kW input rate, but these are not shown here. The defrost process can be subdivided into three stages as follows; (i) temperature inversion of the secondary working fluid upon commencement of defrost, (ii) sensible heating of the heat exchanger, circuit and secondary working fluid, (iii) defrost process consisting of two sub-stages, namely heating of the secondary fluid to 0°C and subsequent frost melting.

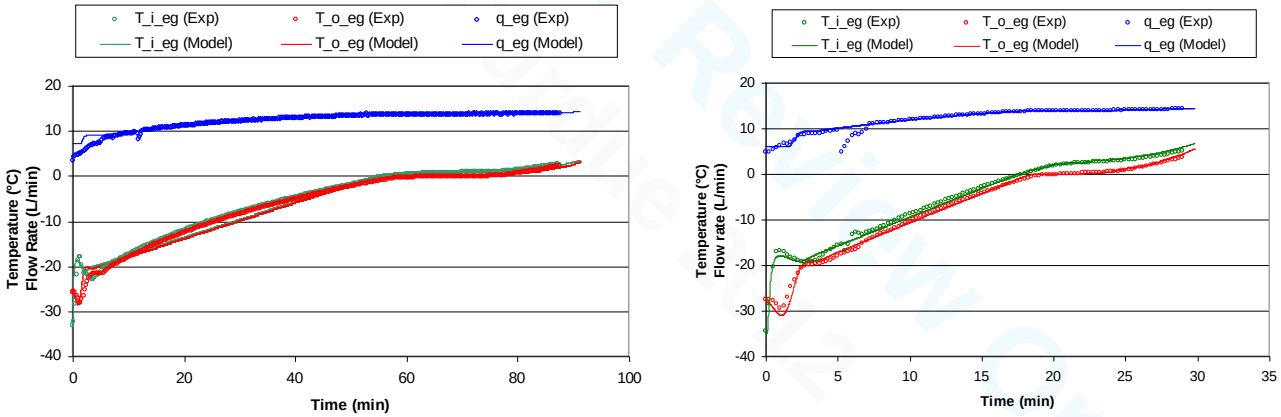

Figure 4: Validation: Electric Defrost Mode (a) 0.5 kW and (b) 2.5 kW

4.2 Hot Gas Defrost

Figure 5 compares model predictions against experimental data for a set-point condition of -20C under hot gas defrost mode. Reasonable prediction of temperature evolution and defrost time is obtained for both cases. Moreover, good model predictions of defrost time are obtained.

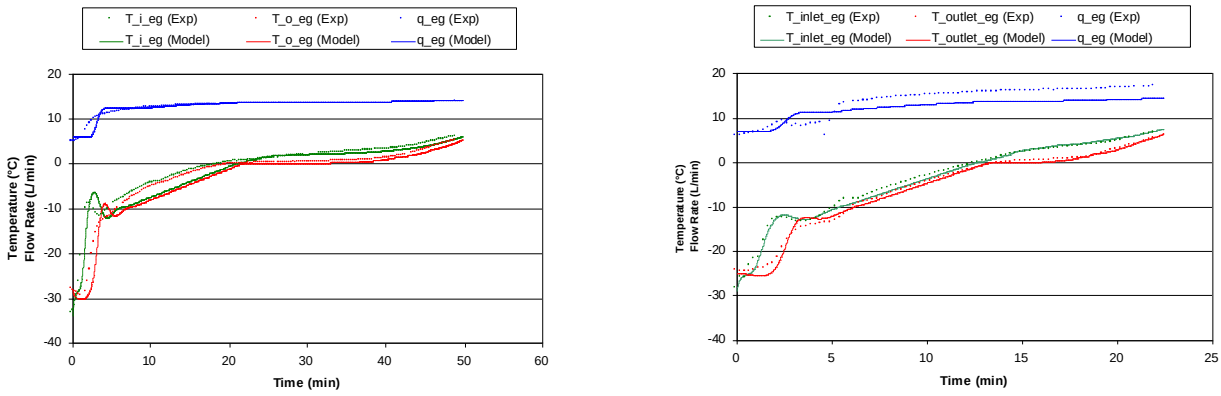

Figure 5: Validation: Hot Gas Defrost Mode (a) 1.5 kW (50Hz) and (b) 3.9 kW (70 Hz)

4.3 Defrost time, Defrost Energy and Defrost Efficiency

Table 2 compares model predictions for defrost time, defrost energy and defrost efficiencies. The key findings are summarised in Figure 6. For hot gas defrost mode, three defrost ratings were used as follows: 1.5 kW, 2.6 kW and 3.9 kW, where each defrost rating was achieved at an inverter controlled compressor frequency of 30, 50 and 70 Hz, respectively. Good agreement is evident for all test conditions as described by the test matrix.

Table 2: Comparison of model and experimental data in terms of defrost time, energy and efficiency

Test	Defrost Method	Defrost Rating (kW) (*Comp. Freq*)	Coldroom Setpoint (°C)	SIMULATION PREDICTIONS			EXPERIMENTAL RESULTS		
				Time (min)	Energy (kJ)	Efficiency (%)	Time (min)	Energy (kJ)	Efficiency (%)
1	Electric	0.5	-20	87.5	2625	40.70	91.2	2737.5	39.02
2	Electric	1.5	-20	38	3420	19.75	38.3	3449.7	19.58
3	Electric	2.5	-20	29	4350	20.27	29.8	4467.0	19.74
4	Hot gas	1.5 (30 Hz)	-20	49	4410	35.02	49.7	4473.0	34.52
5	Hot gas	2.6 (50 Hz)	-20	29.75	4659	21.14	30.1	4705.8	20.93
6	Hot gas	3.9 (70 Hz)	-20	22	5161	17.73	22.4	5262.1	17.39
7	Electric	1.5	-12	35	3150	28	35.9	3228.3	27.32
8	Electric	1.5	-0	21	1890	28	21.3	1915.2	27.63
9	Electric	1.5	-20	28	2520	32.88	28.2	2534.0	32.71

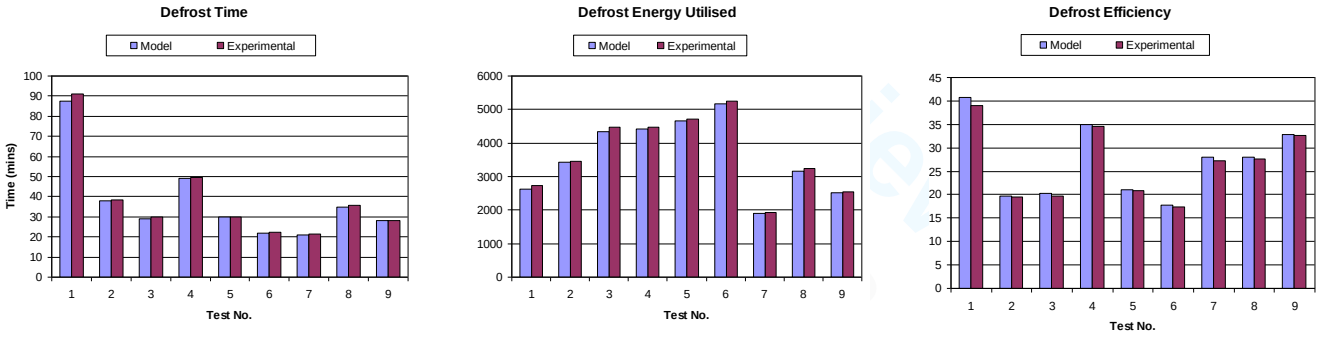

Figure 6: Comparison of model predictions and experimental data for defrost time (s), energy (kJ) and efficiency (%) for Tests 1 to 9 as described in Table 2.

5. SENSITIVITY STUDIES

A series of sensitivity studies were carried out aimed at examining key defrost performance indices as follows: (a) defrost energy distribution, (b) defrost energy utilisation and (c) defrost time. Studies were undertaken for three chamber set point conditions (-20, -10 and 0°C) with associated initial glycol inlet chiller entry temperatures (-30, -22.5, -15°C, respectively). Defrost heat input rates of between 0.5 kW and 5 kW were considered. For initial conditions, a frost mass of 3 kg was assumed with an associated coverage of 100%.

5.1 Defrost Energy Distribution

The total energy utilised during defrost is assumed to be attributed to three components as follows: (i) the secondary working fluid, (ii) the heat exchangers and distribution circuit elements and, (iii) the frost storage. Figure 7 shows the distribution of energy for the 0°C and -20°C defrost cases.

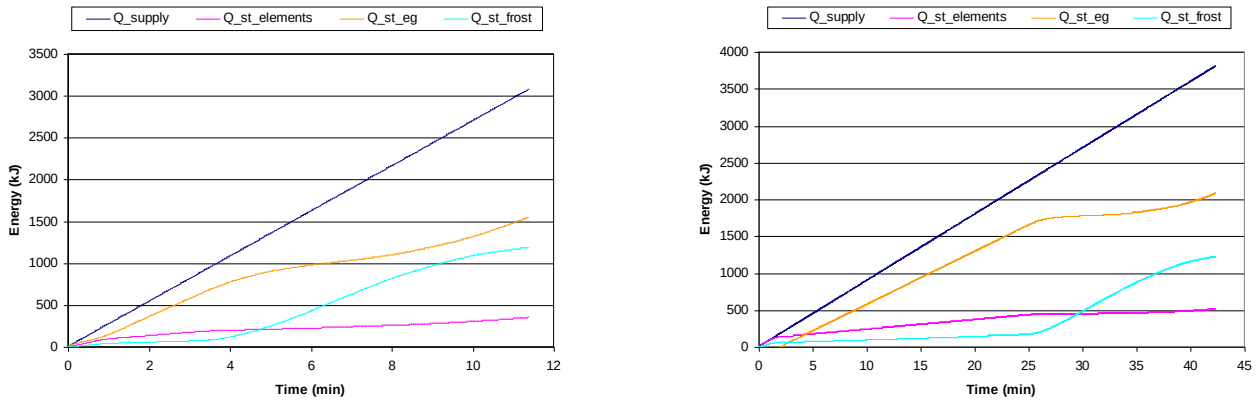

Figure 7: Energy distribution (a) T_room = 0 °C, P_supply = 4.5 kW, (b) T_room = -20°C P_supply = 1.5 kW

A number of observations are made as follows: (a) Supplied Energy: The energy supplied during defrost (Q_supply), is independent of the defrost model behaviour and depends only on the rate of heat input to the secondary working fluid. Therefore its input over time is represented as a constant energy input process, (b) System Stored Energy: The energy stored in the system elements (Q_st_elements, i.e., heater, pipes and chiller tubes and fins) is observed to absorb a steady amount of energy in order to raise its temperature from the initial condition to the temperature associated with the flowing secondary working fluid, (c) Secondary Working Fluid Stored Energy: The profile of the energy stored in the secondary working fluid (Q_st_eg) is observed to increase as the glycol is heated from its initial condition, but to decrease once frost melting occurs as energy is diverted to the frost melt process, (d) Energy stored by the frost (Q_st_frost): The initial energy associated with the melting of the frost is observed to increase steadily as the frost is heated sensibly to it melting point, when the required energy is observed to increase significantly. Furthermore, once frost melting commences, the associated energy with the systems elements and glycol remain steady during defrosting.

5.2 Energy Utilisation

Figure 8 shows the total energy utilised in defrost as a function of the rate of heat input. It can be seen that heat input for all components (except frost melt energy) increases with increasing defrost heat input. Therefore, it would appear, at least from an energy utilisation perspective, that the most energy effective method to carry out defrost is with a reduced power input, if the time required for defrost is not an issue.

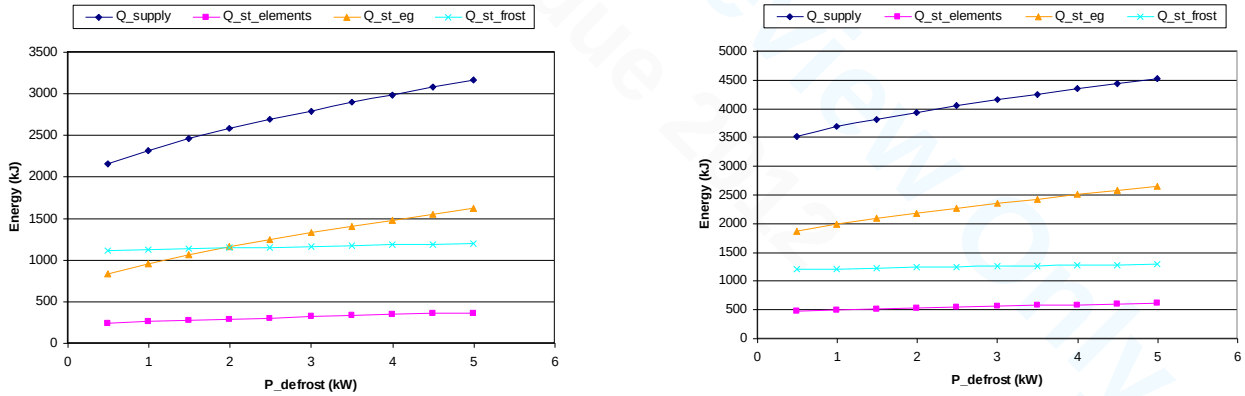

Figure 8: Energy distribution (a) T_room = 0 °C and (b) T_room = -20°C

To assess the additional energy penalty with increasing defrost rating (i.e., from 0.5 kW to 5kW), the effect of different energy defrost ratings is summarised in Table 3. All data is normalized with respect to the lowest defrost power (0.5 kW) using a frost mass of 3 kg.

Table 3: Additional energy penalty as a function of energy utilised for different defrost ratings for an initial frost mass of 3 kg.

Defrost power (kW)	T_room = 0 °C	T_room = -10 °C	T_room = -20 °C
0.5	0 %	0 %	0 %
1.0	7.37 %	5.60 %	4.52 %
1.5	13.64 %	10.36 %	8.36 %
2.0	19.29 %	14.63 %	11.81 %
2.5	24.44 %	18.54 %	14.93 %
3.0	29.27 %	22.24 %	17.95 %
3.5	33.95 %	25.73 %	20.68 %
4.0	38.22 %	29.01 %	23.35 %
4.5	42.58 %	32.29 %	25.97 %
5.0	46.56 %	35.18 %	28.45 %

5.3 Glycol Temperatures

Figure 9 depicts the final glycol temperatures at the end of defrost as a function of heat input rate. The end of defrost is assumed to be when the frost in the "A" node (Fig 3c) has melted, at which point the simulation is terminated. A number of observations can be made as follows. First, the greater defrost heat is, the higher the final glycol temperatures. Second, the difference between the final inlet and outlet temperatures increases with the defrost power. This is consistent with the conclusion extracted from the energy balance, as the energy stored by the glycol increases with defrost power. Third, it is noted that the initial conditions do not appear to affect the final temperatures, being only dependent on the defrost power.

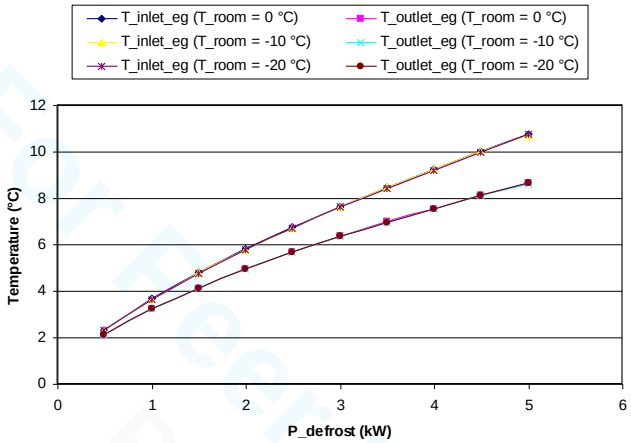

Figure 9: Final glycol temperatures

5.4 Defrost Time and Defrost Efficiency

Defrost time is defined as the time required to complete defrost, and it depends on the initial conditions (temperature, frost mass) and the defrost power input. Figure 10 shows the required defrost time depending on the power supplied for the chamber set points (0, -10 and -20 ºC). It can be seen that as defrost power input is increased, the required defrost time is reduced. As defrost power input is decreased below 1 kW, the time required for defrost is observed to increase significantly. Finally as defrost power increases beyond 3 kW, the observed gain in defrost time is negligible. Defrost efficiency is the relation between the amount of energy that is required to melt the frost, and the total energy supplied to the system during the defrost cycle. Figure 11 shows the efficiency obtained depending on the defrost power used for the three room temperatures considered. The main conclusion is that defrost is most efficient at low temperatures, despite the disadvantages of a higher associated defrost time.

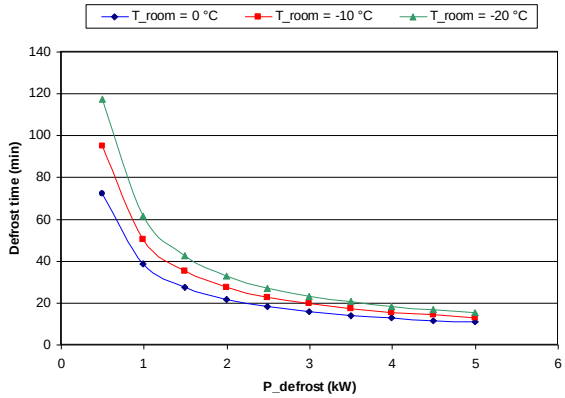

Figure 10: Defrost time

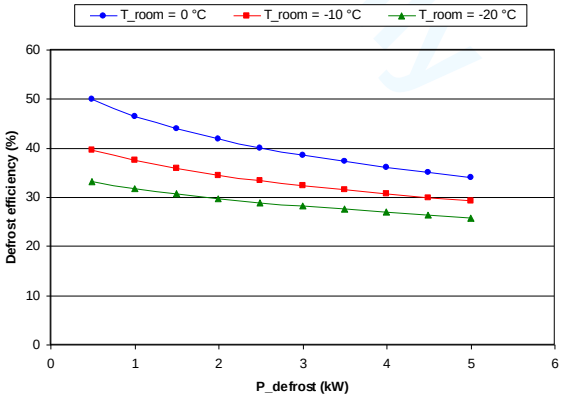

Figure 11: Defrost efficiency

5.5 Frost Density and Mass

For all the results considered to the point, complete frost coverage of the heat exchanger has been assumed. This assumption was motivated by the ease by which this condition could be created in the laboratory for validation studies. In this section the sensitivity of defrost to changes in frost density and frost mass is considered.

Figure 12 considers the defrost process for frost of the same total mass of frost (which is equivalent to change the density of the frost). The results obtained show that little difference is evident between them, except for the last part of the process. It can be observed that the defrost time required to melt the frost is shorter for scenarios where less frost blockage occurs, therefore the efficiency is better for those cases, as the required energy to melt the frost is the same (as the mass of frost is the same).

Figure 13 shows the results of analysis for different amounts of frost on the chiller. The main observable differences are evident in the last part of the process, when active defrost is occurring. The more frost that is present on the chiller from the beginning of defrost, the longer the associated defrost stage. In addition, there is a little effect in the slope of the second defrost stage.

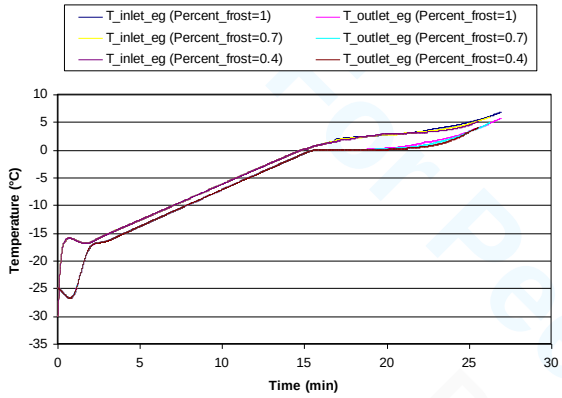

Figure 12: Defrost process as a % of frost

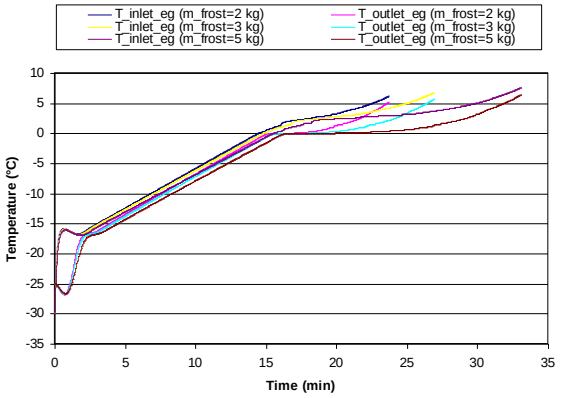

Figure 13: Defrost process as a function of frost mass

6. CONCLUSIONS

A finite difference model of the defrost process in a secondary loop transport refrigeration system is described. The model is validated against experimental data from a series of test for both electric and hot gas defrost mode. Best defrost efficiencies were achieved with the lowest defrost powers, although a much longer defrost time is required. Use of high defrost rates, results in a greater final supplied energy to carry out defrost with up to 50% more energy used compared to lower defrost rates. Other parameters that affect the efficiency of the process is the mass of frost present on the chiller before defrost.

NOMENCLATURE

Variables			Subscripts	
m	mass	(kg)	eg	ethylene glycol
P	defrost power	(W)	heater	electric heater
t	time	(s)	i	inlet
T	temperature	(ºC)	melt_frost	frost melting
q	heat transfer	(W)	o	outlet
			room	cold room

REFERENCES

Alebrahim, A.M and Sherif, S.A 2002. Electric defrosting analysis of a finned-tube evaporator coil using the enthalpy method. *Proc Inst. Mech. Engrs.* Vol. 216 Part C: J. Mechanical Engineering Science, 655-673, (2002).

Aittomaki, A., Lahti, A., 1997, Potassium formate as a secondary refrigerant *Int. J. Refrig.* 20(4) pp276-282.

ATP, 2003, Economic Commission for Europe; Inland Transport Committee Agreement on the International Carriage of Perishable Foodstuffs and on the Special Equipment to be used for such carriage, United Nations Publication *UNECE* Annex 1(3), pp12-34, ISBN 92-1-139089-3.

EES 2008, Engineering Equation Solver. Version 8. www.fChart.com.

Hoffenbecker, N. 2004, Investigation of alternative defrost strategies, *Master Thesis*, Solar Energy Laboratory, University of Wisconsin – Madison, 2004.

Hoffenbecker, N., S.A. Klein, D. T. Reindl, 2005, Hot gas defrost model development and validation, *International Journal of Refrigeration*, January 2005.

Horton, W.T., Groll, E.A., 2003, Secondary Loop Refrigeration in Supermarket Applications – A case study, Paper ICR0345 *Proc. IIF/IIR Int Cong. Refrig.*, Washington DC, USA.

Kazachki, G.S., Hinde, D.K., 2006, Secondary Coolant Systems for Supermarkets *J. ASHRAE*, Sep 06, pp34-46

Krakow, K. L., Van, L. and Lin, S., 1992, A model of hot gas defrosting of evaporator. *Parts I and II, ASHRAE Trans*, Vol. 98, Part 1, 451-474 (1992)

Liu, Z., and Guangfa Tang, F.Z., 2003, Dynamic simulation of air-source heat pump during hot-gas defrost. *Applied Thermal Engineering* 23 (2003) 675–685.

Mago, P.J. and Sherif, S.A. 2002, Dynamics of coil defrosting in supersaturated freezer air *Proc Inst. Mech. Engrs.* Vol. 216 Part C: J. Mechanical Engineering Science, 949-958, (2002).

Mei, V. C., Chen, F. C., Domitrovic, R. E., Braxton, B. D., 2002, Warm liquid defrosting for supermarket refrigerated display cases. *ASHRAE Transactions.* 108(1), 669-674. 2002

Melinder, A., 1997, "Thermophysical properties of liquid secondary refrigerants – Charts and Tables" Published by *IIF/IIR*, Paris, France.

Sawalha, S., Palm, B., 2003, "Energy consumption evaluation of indirect systems with CO2 as a secondary refrigerant in supermarket refrigeration" Paper ICR0434 *Proc. 21st IIF/IIR Int. Cong. Refrig.*, Washington DC, USA

ACKNOWLEDGEMENTS

This research was carried out at University College Dublin by visiting student Andreas Cabellos-Portoles, who was financially supported by the European Union (EU) under the auspices of an Erasmus bi-lateral agreement (LLP 2006/2007) between University College Dublin and Universitat Politècnica de València, Valencia, Spain. The advice of Prof. Jose Miguel Corberán is gratefully acknowledged.